A Quantum Monte Carlo Method for Non-Parabolic Electron Bands in Semiconductor Heterostructures

J Shumway

Department of Physics and Astronomy, Arizona State University, Tempe, AZ, 85287, USA

E-mail: john.shumway@asu.edu

Abstract. We present a many-body computational technique for simulating interacting electrons in non-parabolic semiconductor bands. The technique uses an imaginary time propagator for a non-parabolic electron band that is described by an energy-dependent effective mass. This derivation exploits a mathematical analogy between the kinetic energy with effective mass corrected to first order in energy and the relativistic kinetic energy. The propagator can be used in ground-state and finite temperature quantum Monte Carlo (QMC) algorithms. We give a demonstration of this path integral QMC technique applied to interacting electrons in a self-assembled InGaAs quantum dot.

Submitted to: *J. Phys.: Condens. Matter (22 December 2004)*

PACS numbers: 02.70.Ss, 73.21.La

1. Introduction

The accurate simulation of electron and hole quasiparticles in semiconductor nanostructures is an important challenge in science and engineering. Two demands, which are often in conflict, are the need to accurately simulate interacting quantum particles and the need to accurately represent the individual quasiparticles [1]. When careful treatment of interactions is important, simplified models such as single-band effective mass models allow the use of analytic techniques [2, 3, 4] or quantum Monte Carlo (QMC) simulations [1, 5, 6, 7, 8]. When a high-quality description of material-specific quasiparticle properties is needed, techniques such as $k \cdot p$ theory [9], empirical pseudopotentials [10], or tight-binding models [11] allow accurate single particle simulations. To add many-body correlations to these more complicated quasiparticle models, a common approach is a multi-determinant expansion of the few-body wavefunction [12, 13, 14, 15, 16]. Such expansions are often underconverged [1], and the multi-determinant techniques scale poorly with the number of quasiparticles.

In this work, we derive a technique for extending the capabilities of quantum Monte Carlo techniques. Band non-parabolicity is often the leading correction to single band

effective mass models of electrons, especially in small-bandgap semiconductors [17]. We show that a propogator for electrons with non-parabolic bands can be derived for use in quantum Monte Carlo. We discuss its application in both ground state and finite-temperature QMC algorithms. As a demonstration, we use the techniques to simulate interacting electrons in a self-assembled InGaAs/GaAs quantum dot.

2. Theory: A Non-Parabolic Propagator

In the simplest effective-mass formalism, electrons are assigned an effective mass that is the inverse of the second derivative of the energy, $m^* = (\partial^2 \varepsilon_k / \partial k^2)^{-1}$, evaluated at the conduction band minimum. For low energy electrons, this single-band approximation is appropriate for many semiconductors. For example, the conduction band in GaAs has a singly-degenerate band minimum at the gamma point, with $m^* \approx 0.067 m_e$. For higher energy electrons, the non-parabolicity of the conduction band must be taken into account. One way to accomplish this is by treating the electron effective mass as an energy dependent quantity. For example, the conduction band minimum in GaAs is better described by $\varepsilon(k) = \hbar^2 k^2 / 2m^*(\varepsilon)$, where

$$m^*(\varepsilon) = m_0^*(1 + \alpha\varepsilon), \tag{1}$$

where $\alpha \approx 0.6557$ eV^{-1} is the non-parabolicity parameter, and $m_0^* \equiv m^*(0)$ refers to the mass when $\varepsilon = 0$. From the two-band Kane model [17], the energy scale for non-parabolicty is set by the band gap, E_{gap}, as $\alpha = 1/E_{\text{gap}}$. This expansion can be continued to higher orders in energy. In this paper, we consider only the first order energy corrections to the effective mass, and derive a quantum Monte Carlo technique for the non-parabolic band. Solving for the energy, one finds the standard expression

$$\varepsilon(k) = \frac{1}{2\alpha}\sqrt{1 + \frac{2\alpha\hbar^2 k^2}{m_0^*}} - \frac{1}{2\alpha}. \tag{2}$$

This first-order non-parabolic correction is equivalent to fitting the conduction band minimum to a hyperbola, rather than a parabola.

In QMC algorithms, the kinetic energy enters the simulations through the propagator $G(\boldsymbol{r}, \boldsymbol{r}'; \tau) = \langle \boldsymbol{r} | e^{-\tau H} | \boldsymbol{r}' \rangle$. This propagator is most easily evaluated by expanding in a plane wave basis,

$$\begin{aligned} G(\boldsymbol{r}, \boldsymbol{r}'; \tau) &= \frac{1}{(2\pi)^3} \int \mathrm{d}^3\boldsymbol{k}\ \exp[\mathrm{i}\boldsymbol{k} \cdot (\boldsymbol{r} - \boldsymbol{r}')] \exp[-\tau\varepsilon(|\boldsymbol{k}|)] \\ &= \frac{\exp\left(\frac{\tau}{2\alpha}\right)}{2\pi^2 r} \int_0^\infty \exp\left[-\frac{\tau}{2\alpha}\left(1 + \frac{2\alpha\hbar^2 k^2}{m_0^*}\right)^{\frac{1}{2}}\right] k \sin kr\, \mathrm{d}k, \end{aligned} \tag{3}$$

where $r = |\boldsymbol{r} - \boldsymbol{r}'|$. This integral also occurs in the evaluation of the real-space propagator of a relativistic free particle [18]. In fact, the hyperbolic dispersion relation in equation (2) is mathematically analogous to the kinetic energy of a relativistic particle. In closed form, the propagator is

$$G(\boldsymbol{r}, \boldsymbol{r}'; \tau) = \frac{\exp\left(\frac{\tau}{2\alpha}\right)\tau}{32\pi^2\alpha z}\left(\frac{2m_0^*}{\hbar^2\alpha}\right)^{\frac{3}{2}} K_2(z), \tag{4}$$

where K_2 is a modified Bessel function of the second kind [19] and

$$z = \frac{\tau}{2\alpha}\left(1 + \frac{2m_0^*\alpha|\boldsymbol{r}-\boldsymbol{r}'|^2}{\hbar^2\tau^2}\right)^{\frac{1}{2}}. \tag{5}$$

We can verify that this propagator has the correct parabolic-band limit: For large $\tau \gg m_0^*|\boldsymbol{r}-\boldsymbol{r}'|^2/2\hbar^2\tau$, expand

$$z \approx \frac{\tau}{2\alpha} + \frac{m_0^*|\boldsymbol{r}-\boldsymbol{r}'|^2}{2\hbar^2\tau}. \tag{6}$$

Using the asymptotic form of the modified Bessel functions, $K_\nu(z) \approx \sqrt{\pi/2z}\exp(-z)$, we find the parabolic band limit,

$$G_0(\boldsymbol{r},\boldsymbol{r}';\tau) = \left(\frac{m_0^*}{2\pi\hbar^2\tau}\right)^{\frac{3}{2}} \exp\left(-\frac{m_0^*|\boldsymbol{r}-\boldsymbol{r}'|}{2\hbar^2\tau}\right). \tag{7}$$

Note that this limit requires two conditions: the distance $|\boldsymbol{r}-\boldsymbol{r}'|$ must be small enough that $\tau \gg m_0^*|\boldsymbol{r}-\boldsymbol{r}'|^2/2\hbar^2\tau$ is satisfied, and $\tau \gg 2\alpha$.

In figure 1 we compare the parabolic-band propagator, G_0, and the hyperbolic-band propagator, G. We have plotted the action, $S = -\ln G$, for a timestep appropriate for QMC simulations of nanostructures, $\tau = 8\ \mathrm{Ha}^{-1} = 4.6 \times 10^{-3}\ \mathrm{eV}^{-1}$. For the parabolic-band propagator, the action is also parabolic, leading to a Gaussian form for G_0. For the hyperbolic-band propagator, we see that the action is diminished at both small and large distances. This leads to a propagator, $G(\boldsymbol{r},\boldsymbol{r}';\tau)$, that, compared to a Gaussian, has a narrower central peak and longer, exponentially decaying tails. For both the parabolic and hyperbolic bands, the normalization of the propagator is unity, and the root-mean-squared width, $\sigma = \sqrt{\langle|\boldsymbol{r}-\boldsymbol{r}'|^2\rangle}$, is equal to $\hbar\sqrt{\tau/m_0^*}$.

3. Simulation Technique

Real-space QMC techniques can be used to simulate correlated electrons in semiconductor nanostructures. For ground state simulations, diffusion QMC propagates the electrons along random walks that project out the ground state energy of the system. For finite temperature, path integral QMC samples the quantum partition function represented as a Feynman path integral. We can use this hyperbolic-band propagator with both types of QMC algorithms, as discussed in this section.

3.1. Diffusion Quantum Monte Carlo

In diffusion QMC, the electrons are propagated in a branching random walk [20]. In the simplest formulation, one moves walkers with the free-particle propagator, then weights the walkers with a factor $\mathrm{e}^{-\tau V(\boldsymbol{R})}$. To sample the hyperbolic-band propagator, one can tabulate a function $f(r)$ defined by

$$(2\pi)^{-\frac{3}{2}} \int_0^r \exp\left(-\frac{r^2}{2}\right) 4\pi r^2\,\mathrm{d}r = \int_0^{f(r)} G(r;\tau) 4\pi r^2\,\mathrm{d}r. \tag{8}$$

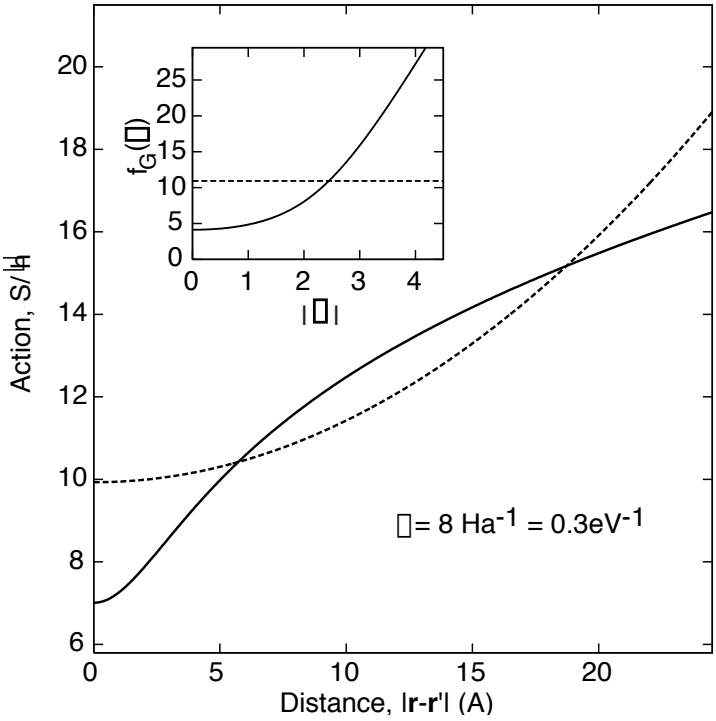

Figure 1. The kinetic action for propagating an electron in GaAs ($m* = 0.067$) for $\tau = 0.8$ Ha^{-1} in imaginary-time. Solid line includes band non-parabolicy $\alpha = 0.6557$ eV^{-1}, while the dashed line shows the parabolic action. Inset shows the scale functions for sampling these propagators from a 3-d Gaussian variate $\boldsymbol{\chi}$, defined in (8).

From a vector $\boldsymbol{\chi}$ drawn from a Gaussian with unit varience, the vector $\boldsymbol{\Delta r} = \boldsymbol{\chi} f(|\boldsymbol{\chi}|)$ samples the hyperbolic-band propagator.

The efficiency and stability of diffusion QMC is often improved by importance sampling with a trial wavefunction Ψ_T. This leads to a drifted random walk and weighting of walkers based on the trial wavefunction. The hyperbolic-band energy, (2), complicates this importance sampling. In this paper, we do not consider importance-sampled diffusion QMC, but instead focus on the path integral QMC method, described next. Some issues for ground state QMC calculations with this hyperbolic-band propagator have been dealt with in relativistic simulations of nuclear models [18, 21, 22].

3.2. Path Integral Quantum Monte Carlo

The thermal density matrix may be written as a sum over paths,

$$\rho(\boldsymbol{R}, \boldsymbol{R}'; \tau) = \int \mathcal{D}R(t) \, \exp(-S[R(t)]), \tag{9}$$

where the path $\boldsymbol{R}(t)$ starts at $\boldsymbol{R}(0) = \boldsymbol{R}'$ and ends at $\boldsymbol{R}(\beta) = \boldsymbol{R}$. For numerical evaluation, the path is discretized into many short intervals with timestep τ, and the action is evaluated for each short interval. Monte Carlo integration may then be used to sample the path integral in order to calculate quantum and thermal averages. For more details of the path integral QMC technique, see the review article by Ceperley [23].

The hyperbolic-band propagator makes a contribution to the action,

$$S(\boldsymbol{r},\boldsymbol{r}';\tau) = -\frac{\tau}{2\alpha} + \ln\left(32\pi^2\alpha z/\tau\right) - \frac{3}{2}\ln\left(\frac{2m^*}{\hbar^2\alpha}\right) - \ln K_2(z). \tag{10}$$

The estimation of energy involves a tau derivative [23],

$$\dot{S}(\boldsymbol{r},\boldsymbol{r}';\tau) = -\frac{1}{2\alpha} - \frac{1}{\tau} + \frac{\tau}{2\alpha^2 z^2} + \frac{\tau}{8\alpha^2 z}\frac{K_1(z)+K_3(z)}{K_2(z)}. \tag{11}$$

A key step in the Monte Carlo sampling of a new path configuration is the sampling of a midpoint of a time interval [23]. If a free particle is at point $\boldsymbol{r}_{i-1}$ at an earlier imaginary time $-\tau$ and is at a point $\boldsymbol{r}_{i+1}$ at a later imaginary time τ, its current position $\boldsymbol{r}$ has the normalized distribution

$$P(\boldsymbol{r}_i) = G(\boldsymbol{r}_{i+1},\boldsymbol{r}_i;\tau)G(\boldsymbol{r}_i,\boldsymbol{r}_{i-1};\tau)/G(\boldsymbol{r}_{i+1},\boldsymbol{r}_{i-1};2\tau). \tag{12}$$

(Recall that the convolution of two Green's functions is $G(\boldsymbol{r}_{i+1},\boldsymbol{r}_{i-1};2\tau) = \int G(\boldsymbol{r}_{i+1},\boldsymbol{r}_i;\tau)G(\boldsymbol{r}_i,\boldsymbol{r}_{i-1};\tau),\mathrm{d}\boldsymbol{r}_i.$) For large times $\tau \gg \alpha$, this is a product of two Gaussians, which is a Gaussian centered between $\boldsymbol{r}_{i-1}$ and $\boldsymbol{r}_{i+1}$. At smaller times, this function is bimodal, with peaks centered around $\boldsymbol{r}_{i-1}$ and $\boldsymbol{r}_{i+1}$.

To sample this joint probability distribution, we use a rejection technique. As an envelope, we sample a point $\boldsymbol{r}_i$ from a normalized sum of two distributions centered around the points $\boldsymbol{r}_{i-1}$ and $\boldsymbol{r}_{i+1}$,

$$P_{2G}(\boldsymbol{r}_i) = [G(\boldsymbol{r}_i,\boldsymbol{r}_{i-1};\tau) + G(\boldsymbol{r}_i,\boldsymbol{r}_{i+1};\tau)]/2. \tag{13}$$

The point is accepted with probability $cP(\boldsymbol{r}_i)/P_{2G}(\boldsymbol{r}_i)$, where c is a constant that keep this probability less than or equal to one at all points. In practice, we find that c can be determined by examining the point $\boldsymbol{r}_i = \boldsymbol{r}_{i-1}$. The rejection rate is very reasonable, typically one-third of points are accepted. In our simulations, we have collected statistics on c and found it to have an average of 0.32 with a sharp peak at a median value of 0.30. Small values of c that would cause many rejections and dramatically slow down the simulation are extremely rare. For example, in a random set of ten thousand values, the smallest value of c was slightly larger than 0.02.

4. Application: Path Integral Simulation of a Heteroepitaxial Quantum Dot

As a demonstration of the technique, we apply it to two electrons in an InGaAs/GaAs self-assembled dot. The non-parabolic effects are significant in this system, and we can nominally compare these calculations to our earlier pseudopotential calculations [24]. A disadvantage of this choice is that the effect of electron-electron interactions are fairly trivial. In these small quantum dots, correlation between two electrons is nearly insignificant relative to first-order perturbative corrections [1]. Correlation does become important in single-dot spectroscopy [1], but inclusion of holes in the calculations introduces other issues that we discuss in the conclusion. Since our focus here is on the improved modeling of electron quasi-particles in QMC simulations, we are content

with studying the small-but-calculable effects of band-nonparabolicity on the interacting electron energies.

In reference [24], a series of quantum dot models with varying size and composition are compared with experimental measurements of size, shape, composition, and photoluminescence spectra. For simplicity, we now focus on one of these model dots: a uniform, conical-shaped dot, with nominal alloy composition of $In_{0.5}Ga_{0.5}As$, having a height of 3.5 nm with a 20 nm base and 16 nm top, and sitting on a 1.85 nm $In_{0.3}Ga_{0.7}As$ wetting layer [24]. As in reference [24], we have calculated the strained band-offsets for electron confinement, using an atomistic valence-force-field model for the strain calculations [25]. The single electron ground state energy as calculated by an empirical pseudopotential technique is 1.420 eV. We have checked that energy using a constant effective mass of $m^* = 0.067$ and a plane wave basis, as shown in table 1. (In this study we have kept the mass independent of position for simplicity. As discussed in reference [26], this approximation is justified because the strain, Ga incorporation, and even the band-nonparabolicity effects in the dot all raise the smaller InAs effective mass to a value much closer to bulk GaAs. Note in particular that the smaller band-gap in the dot would increase the non-parabolicity factor beyond the constant value we are using, partially offsetting the smaller InGaAs effective mass in the dot.) With parabolic bands, the effective mass ground state energy is 1.429 eV, and with non-parabolic bands this energy drops to 1.415 eV.

We have run path integral QMC simulations for one and two electrons in the dot. For one electron, we find that the parabolic and non-parabolic models give very close agreement between the path integral simulation and the plane-wave calculation, as summarized in table 1. This close agreement is very compelling evidence that our Monte Carlo implementation of the non-parabolic propagator is in fact able to model the non-parabolic bands accurately. In the second row of the table, we show coulomb energy corrections within first-order perturbation theory, using a dielectric constant $\epsilon = 13$, and the total energies within perturbation theory is shown in in the third row. The small differences in absolute values off the perturbative corrections for different methods are like due to differences in real-space integration techniques. The fact that the pseudopotential coulomb correction is smaller than the correction obtained with effective mass may also be due to incomplete convergence of the "linear combination of bulk-bands" basis [27] used with the pseudopotential hamiltonian [24].

The path integral simulations can directly solve this interacting two-particle system, as shown in the bottom line of the table. To add electron-electron interactions to the action, we tabulated the pair coulomb density matrix on a radial grid with a 4th order polynomial expansion for the off-diagonal coordinate [23], using the analytic expansions of Vieillefosse [28]. (We make an additional approximation of using the pair coulomb density matrix as calculated with parabolic kinetic energy, even when simulating non-parabolic bands.) The improvements beyond first-order perturbation theory in the path integral calculations include both self-consistency corrections and correlation. For the parabolic effective-mass calculations, the change is small, about -0.7 ± 0.3 meV. For non-

Table 1. Energies for one- and two- electrons in an InGaAs dot, in eV, measured from the bulk GaAs valence band edge. Pseudopotential calculations incorporate complete band structure, and are used to check our effective-mass-approximation (EMA) calculations with parabolic ($\alpha = 0$) and non-parabolic ($\alpha > 0$) bands. Total energies include correlation and self-consistent interactions, which we compared with perturbation theory (PT).

		Plane Wave EMA		Path Integral[a] EMA		
N_e	quantity	Pseudopotentials[b]	($\alpha = 0$)	($\alpha = E_{\rm gap}^{-1}$)	($\alpha = 0$)	($\alpha = E_{\rm gap}^{-1}$)
1	total energy	1.420	1.4289	1.4153	1.4293(1)	1.4143(3)
2	PT shift	0.021	0.021	0.023	0.023	0.025
2	PT total	2.861	2.879	2.854	2.8807(2)	2.8536(6)
2	total energy	—	—	—	2.8800(2)	2.8509(5)

[a] Statistical errors in last digit of Monte Carlo integrations are shown in parenthesis.
[b] Empirical pseudopotential calculation results from Ref. [24].

parabolic effective mass calculations, the change is significantly larger, about -2.7 ± 0.8 meV. This is the expected trend: the non-parabolicity softens up the wavefunction, allowing larger self-consistent corrections and more correlation. This is completely analogous to relativistic-kinetic-energy corrections in atomic physics. The effect can also be understood from perturbation theory: the non-parabolicity significantly lowers the energies of excited states, enhancing higher-order perturbative corrections.

5. Conclusion

We have shown a method for including the effects of non-parabolic bands in QMC simulations of semiconductor nanostructures. Tests on a InGaAs quantum dot show that the inclusion of non-parabolicity brings the effective mass calculations in closer agreement to single-electron energies as calculated by empirical pseudopotentials. While this demonstration focused on two electrons, we note that the quantum Monte Carlo formalism can be extended to many electrons with an additional fixed-node approximation [8]. The algorithmic improvements we have described here should have immediate applications to current QMC simulations of self assembled dots and enable more realistic simulations of two-dimensional electron gasses in real semiconductor heterostructures.

Future work will consider improvement in the simulation of hole states. For strained heterostructures, such as the InGaAs quantum dot considered here, strain breaks the degeneracy of the hole band. These strained holes are sometimes approximated with single-band anisotropic effective masses [2]. In that case, the non-parabolic effects are accompanied by mixing of other hole bands, so the technique described here is not applicable. Rather, techniques that include degrees of freedom for the internal spin and band indices for holes will be necessary to go beyond the parabolic mass approximation

for holes.

Acknowledgments

The author thanks Kevin Schmidt for helpful discussions. Work supported by NSF grant DMR 02-39819.

References

[1] Shumway J, Franceschetti A and Zunger A 2001 *Phys. Rev. B* **63** 155316
[2] Jacak L, Wójs A and Harylack P 1998 *Quantum Dots* (Berlin: Spinger-Verlag)
[3] Yannouleas C and Landman U 2002 *J. Phys.: Condens. Matter* **14** L591
[4] Serra L, Nazmitdinov R G and Puente A 2003 *Phys. Rev. B* **68** 035348
[5] Bolton F 1996 *Phys. Rev. B* **54** 4780
[6] Lee E, Puzder A, Chou M Y, Uzer T and Farrelly D 1998 *Phys. Rev. B* **57** 12281
[7] Harting J, Mülken O, and Borrmann P 2000 *Phys. Rev. B* **62** 10207
[8] Shumway J, Fonseca L R C, Leburton J P, Martin R M and Ceperley D M 2000 *Physica E* **8** 260
[9] Bimberg D, Grundman M and Ledentsov N N 1999 *Quantum Dots Heterostructures* (New York: John Wiley & Sons)
[10] Williamson A J, Wang L W and Zunger A 2000 *Phys. Rev. B* **62** 12963
[11] Lee S, Jönsson L, Wilkins J W, Bryant G W and Klimeck G 2002 *Phys. Rev. B* **63** 235307
[12] Dekel E, Gershoni D, Ehrenfreund E, Spektor D, García J M and Petroff P M 1998 *Phys. Rev. Lett.* **80** 4991
[13] Barenco A and Dupertuis M A 1995 *Phys. Rev. B* **52** 2766
[14] Franceschetti A, Fu H, Wang L W and Zunger A 1999 *Phys. Rev. B* **60** 1819
[15] Williamson A J, Franceschetti A and Zunger A 2001 *Europhys. Lett.* **53** 59
[16] Guffarth F, Heitz R, Schliwa A, Stier O, Geller M, Kapteyn C M A, Sellin R and Bimberg D 2003 *Phys. Rev. B* **67** 235304
[17] Kane E O 1957 *J. Phys. Chem. Solids* **1** 249
[18] Carlson J, Heller L and Tjon J A 1988 *Phys. Rev. D* **37** 744
[19] Abramowitz M and Stegun I 1970 *Handbook of Mathematical Functions* (New York: Dover Publications, Inc.)
[20] Foulkes W M C, Mitas L, Needs R J and Rajagopal G 2001 *Rev. Mod. Phys.* **73** 33
[21] Carlson J and Pandharipande V R 1991 *Phys. Rev. D* **43** 1652
[22] Carlson J, Pandharipande V R and Schiavilla R 1993 *Phys. Rev. C* **47** 484
[23] Ceperley D M 1995 *Rev. Mod. Phys.* **67** 279
[24] Shumway J, Williamson A J, Zunger A, Passaseo A, DeGiorgi M, Cingolani R, Catalano M and Crozier P 2001 *Phys. Rev. B* **64** 125302
[25] Martin R M 1970 *Phys. Rev. B* **1** 4005
[26] Wójs A, Hawrylak P, Fafard S and Jacak L 1996 *Phys. Rev. B* **54** 5604
[27] Wang L W and Zunger A 1999 *Phys. Rev. B* **59** 15806
[28] Vieillefosse P 1994 *J. Stat. Phys.* **80** 461